Cochlea-Based RF Channelizing Filters

Christopher J. Galbraith, *Student Member, IEEE*, Robert D. White, *Member, IEEE*, Lei Cheng, Karl Grosh, and Gabriel M. Rebeiz, *Fellow, IEEE*

***Abstract*—A new type of contiguous-channel RF multiplexing filter has been developed. The filter topology is derived from an electrical–mechanical analogy of the mammalian cochlea, and this channelizer retains the desirable features of the cochlea including multiple-octave frequency coverage, a large number of output channels, and an enhanced high-order upper stop-band response. Results of two 20-channel, 20–90-MHz channelizer prototypes, one with constant fractional bandwidth channels and another with constant absolute bandwidth channels, are presented and agree well with theory.**

***Index Terms*—Channelizer, cochlea, filter, manifold, multiplexer.**

I. Introduction

RADIO frequency (RF) multiplexers with a large number of output ports—called *channelizers*—have always posed a challenging design problem. Standard multiplexer designs use a set of channel filters connected by a manifold consisting of transmission lines (or waveguide) and tuning elements between separate channel filters. Waveguide-based solutions require extensive manual tuning and are bulky and expensive, but offer excellent performance [1]. Several planar manifold multiplexers, using both conventional and superconducting technologies, have also been demonstrated with varying degrees of manifold complexity, size, and optimization requirements. Of particular note, a logarithmic-periodic microstrip multiplexer with contiguous channels and a straightforward design procedure was made at C- and X-bands [2].

This study presents a different approach to planar manifold channelizer design where the channelizer circuit is obtained from an electrical–mechanical analogy of a cochlear model. This biologically inspired multiplexer uses interactions among channel filters to produce a high-order upper stop-band response, even with single resonator channel filters. The needed channel interaction is provided by a low-value series inductance between adjacent channel filters resulting in a compact physical layout, a simple design procedure, and an unlimited number of channels. Because the channelizer is completely passive, it offers excellent linearity and zero dc power consumption.

Manuscript received October 10, 2006; revised July 6, 2007. The work was supported by the U.S. Air Force under Contract FA8721-05-C-0002. This paper was recommended by Associate Editor G. Cauwenberghs.

C. J. Galbraith is with the Radiation Laboratory, Department of Electrical Engineering and Computer Science, The University of Michigan, Ann Arbor, MI 48109 USA (e-mail: cgalbrai@umich.edu).

R. D. White is with the Mechanical Engineering Department, Tufts University, Medford, MA 02155 USA (e-mail: r.white@tufts.edu).

L. Cheng and K. Grosh are with the Mechanical Engineering Department, The University of Michigan, Ann Arbor, MI 48109 USA (e-mail: lchengz@umich.edu and grosh@umich.edu).

G. M. Rebeiz is with the Electrical and Computer Engineering Department, University of California at San Diego, La Jolla, CA 92037 USA (e-mail: rebeiz@ece.ucsd.edu).

Digital Object Identifier 10.1109/TCSI.2008.916537

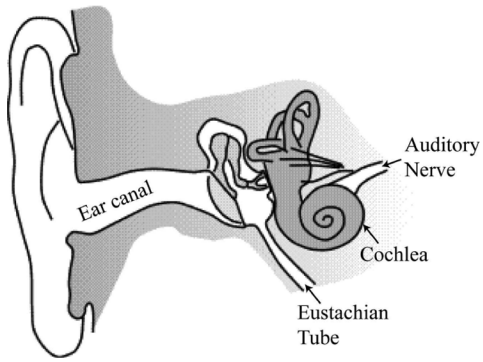

Fig. 1. Periphery of the human auditory system. The basilar membrane is contained within the cochlea.

A cochlear-inspired passive RF channelizer was first reported in [3]. In this work, the 20–90-MHz band was covered with 20 contiguous channels, each with a constant fractional bandwidth. This paper expands on the original work by presenting the complete theory and design procedure for both fractional and constant bandwidth channelizers and the results of an additional channelizer design with constant absolute bandwidth channels. In addition, the time-domain behavior of these channelizers is examined.

Applications of this channelizing filter include wideband, contiguous-channel receivers for signal intelligence or spectral analysis. In its simplest form, the channelizing filter is used to decompose a wideband input signal into contiguous channels, whose outputs are then fed to separate amplifiers, mixers, and detectors, providing simultaneous reception over the entire input bandwidth. By using a less complex receiver chain (for instance, an envelope detector) at each filter output, this wideband receiver becomes a spectrum analyzer.

II. Motivation: The Cochlea

The cochlea is the electro-mechanical transducer located in the inner ear that converts acoustical energy (sound waves) into nerve impulses sent to the brain (Fig. 1). The cochlea is an amazing channelizing filter with approximately 3000 distinct channels covering a three-decade frequency range and can distinguish frequencies that differ by less than 0.5% [4], [5].

The filtering characteristics of the cochlea rely on the propagation of a coupled fluid-structure wave that results in a localized spatial response for each frequency. In the biological cochlea, active processes enhance the frequency response of the system; we only consider the basic hypothesis for how the passive system works. The structure (the basilar membrane and organ of Corti) can be thought of as a flexible membrane comprised of a series

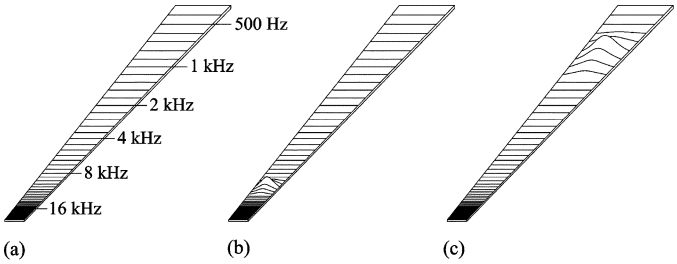

Fig. 2. (a) "Unwound" basilar membrane acts as a continuum of resonant beams, shown with input signals of (b) high frequency and (c) low frequency.

of parallel beams upon which a fluid rests (Fig. 2). In the biological cochlea and in the unwound idealization, acoustic input occurs closest to the narrowest beams at the stapes (or footplate). Other than the stapes and the flexible membrane, the fluid is acoustically trapped. The stapes vibration excites the cochlear fluid which in turn gives rise to a structural acoustic traveling wave down the length of the flexible membrane. Because the resonant frequencies of the flexible membrane are organized from high frequency (where the acoustic information is input) to low frequency, the spatial response of the membrane is frequency selective and spatially organized with the peak of the response occurring at different locations for different frequencies. Specialized cells called inner hair cells are arrayed down the length of the cochlea. These cells rate encode firing of the auditory nerve to the amplitude of the fluid motion [6].

To the best of our knowledge, the work presented here is the first attempt to create a passive RF channelizing filter using a model derived from cochlear mechanics. Previous efforts on achieving cochlear-like filtering have focused on using very large-scale integration (VLSI) techniques to implement active circuit realizations of a cochlear-mechanics model at audio frequencies [7], [8]. More recently, high-frequency integrated circuit techniques and network synthesis of cochlea-like active filters have ben used to extend active cochleas to RF and microwave frequencies [9], [10]. In contrast, the work presented here is passive and uses shunt-connected resonators coupled by series inductors to create a cochlea-like response.

III. Cochlear Modeling

In the simplest mechanical model of the cochlea, a one-dimensional (1-D) fluid interacts with a variable impedance locally reacting structure. The impedance of this structure can be expressed as a function of its mass (m), damping (r), and stiffness (k), where all parameters are functions of position along the structure and are expressed per unit area as

$$Z(x) = j\omega m(x) + r(x) + \frac{k(x)}{j\omega} = \frac{-P(x)}{v_{bm}(x)} \tag{1}$$

where $P(x)$ is the fluid pressure immediately above the structure (at $z = 0$) and v_{bm} is the structure velocity. An inviscid, incompressible, 1-D fluid model produces a simple relationship between pressure and membrane velocity

$$\frac{d^2P(x)}{dx^2} = -j\omega\frac{\rho}{H}\, v_{bm}(x) \tag{2}$$

where ρ is the fluid density and H is the duct height. Eliminating v_{bm} from (1) and (2) and rearranging yields an equation for the basilar membrane pressure

$$\frac{d^2P(x)}{dx^2} + \frac{\frac{\rho}{Hk(x)}}{1 + j\omega\frac{r(x)}{k(x)} - \omega^2\frac{m(x)}{k(x)}}\omega^2 P(x) = 0. \tag{3}$$

This is a highly dispersive waveguide problem, where the coupled effects of the mechanical membrane and the fluid loading create the dispersion relation. Structural acoustic waves traveling along the basilar membrane experience a delay relative to the input, with a phase velocity that varies as a function of position as well as frequency. As the traveling wave approaches the resonant section of the membrane, wave velocity decreases rapidly and the wave ceases to propagate. Further, since the membrane properties change slowly with respect to wavelength, little energy is reflected back to the input. In effect, the basilar membrane acts as a dispersive delay line for traveling structural acoustic waves, with a spatially-dependent cutoff frequency.

A. Mechanical–Electrical Analogy

The equation of motion in the mechanical domain given by (3) can be rewritten in terms of electrical parameters by using a mechanical–electrical analogy. In general, there is a choice regarding the relationship between mechanical and electrical parameters, although several physically meaningful analogies are common. In this case, we replace basilar membrane fluid pressure (P) in the mechanical domain with voltage (V) in the electrical domain

$$V(x) \longleftrightarrow P(x). \tag{4}$$

Other substitutions follow from this choice, including

$$\begin{aligned} L_2(x) &\longleftrightarrow m(x) \\ C(x) &\longleftrightarrow \frac{1}{k(x)} \\ R(x) &\longleftrightarrow r(x) \\ L_1(x) &\longleftrightarrow \frac{\rho}{H}. \end{aligned} \tag{5}$$

The result of this analogy is an equation of motion in the electrical domain given by

$$\frac{d^2V(x)}{dx^2} + \frac{L_1(x)C(x)}{1 + j\omega R(x)C(x) - \omega^2 L_2(x)C(x)}\omega^2\, V(x) = 0 \tag{6}$$

where V is the voltage along the transmission line, L_1 and C are the series inductance and shunt capacitance per unit length, $1/R$ is the shunt conductance per unit length, and $1/\omega L_2$ is the shunt inductive susceptance per unit length. For the discrete lumped-element model, these lead to component values based on the level of discretization, as shown in Fig. 3. Note that V, L_1, L_2, C, and R are functions of position along the transmission line.

In the analogy to the mechanical model, the series inductance L_1 plays the role of the fluid coupling while the shunt resonator elements L_2, C, and R play the role of the variable impedance structure. For this model, the variable x describes a normalized

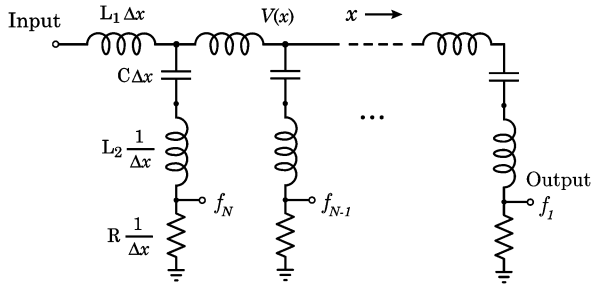

Fig. 3. Discretized transmission-line model of the mammalian cochlea.

position along the circuit, where $x = 0$ corresponds to the circuit input and $x = 1$ refers to the location immediately to the left of the final channelizer section. In terms of channel number n, the channelizer input refers to $n = N$ (highest frequency) while the last channel corresponds to $n = 1$ (lowest frequency), so that

$$x = 1 - \frac{n}{N}, \qquad 0 \le x \le 1, \quad 1 \le n \le N.$$

The channelizer operates as a low-pass transmission-line structure shunt-loaded by series-resonator sections. Each resonator appears as a short-circuit at its resonant frequency and an open-circuit off resonance. The highest frequency channel resonator is located *closest* to the input while the lowest frequency channel is located at the end of the transmission line. Since the highest frequency components are removed from the input signal first, the rejection on each channel's upper side is much steeper than on the lower side. This response is characteristic of mammalian cochleas and is demonstrated later in simulated and measured results.

IV. Channelizer Circuit Design

To arrive at an actual channelizer design, we must choose the element values for the cochlea-like circuit described by (6). For this, we rely on earlier modeling efforts for the case of a channelizer whose channels have a constant fractional bandwidth. An alteration of this model allows the design of constant absolute bandwidth filters described later.

A. Constant Fractional Bandwidth Formulation

In a constant fractional bandwidth channelizing filter, each filter section has the property

$$\frac{\Delta f}{f_0} \equiv \frac{1}{Q} = \text{constant} \tag{7}$$

where f_0 and Δf are the center frequency and bandwidth of a particular channel, and Q is approximately the loaded quality factor of the series resonant circuit channel filter; the channel filter's actual Q is slightly lower due to the loading of adjacent channels. The channel bandwidth definition used in this design is the difference in (upper and lower) passband frequencies where adjacent channel transmission responses cross each other. For a channelizer with constant fractional bandwidth channels, the functional dependence between the coefficients in (3) and (6) is given by [11] and [12]. Written in terms of the channelizer circuit elements, these relations are

$$L_2(x)C(x) = A_1 e^{\alpha x} \tag{8}$$

$$R(x)C(x) = A_2 e^{0.5\alpha x} \tag{9}$$

$$L_1(x)C(x) = A_3 e^{\alpha x}. \tag{10}$$

Note that (8)–(10) define an exponential scaling of resonator component values required to implement series resonator channels with a constant fractional bandwidth. In these functions, A_1, A_2, A_3, and α are constants to be determined, while L_1, L_2, C, and R are the desired channelizer circuit elements. Using (8), the series resonator branches have a resonant frequency given by

$$f_0 = \frac{1}{2\pi\sqrt{L_2(x)C(x)}} = \frac{1}{2\pi\sqrt{A_1 e^{\alpha x}}} \tag{11}$$

so that their resonant frequencies decrease exponentially as we go from left (input) to right along the channelizer circuit. Also, note that the loaded Q of each series LCR resonator can be written as

$$Q = \frac{X}{R} = \frac{2\pi f_0 L_2}{R} = \frac{1}{R(x)}\sqrt{\frac{L_2(x)}{C(x)}} \tag{12}$$

so that, by using (8) and (9) in (12), we find that each resonator has an identical loaded Q, where

$$Q = \frac{\sqrt{A_1}}{A_2}. \tag{13}$$

Since the fractional bandwidth of each resonator is just the reciprocal of the loaded Q, the functional dependence of (8)–(10) results in a channelizer whose channels exhibit a constant fractional bandwidth.

The number of channels N needed can be estimated as a function of the desired total bandwidth with a given channel fractional bandwidth. First, consider two adjacent channels, each crossing over at 2 dB below each channel's identical maximum transmission value. The two channels' center frequencies are related by

$$f_{n+1} = f_n + \frac{\Delta f_{n+1}}{2} + \frac{\Delta f_n}{2}, \qquad 1 \le n \le N. \tag{14}$$

Using (7) to write Δf in terms of fractional bandwidth $(1/Q)$, this becomes

$$\frac{f_{n+1}}{f_n} = \frac{1 + 1/2Q}{1 - 1/2Q}. \tag{15}$$

For an N-channel channelizer, the maximum and minimum frequencies are related by

$$\frac{f_{\max}}{f_{\min}} = \frac{f_N}{f_1} = \left(\frac{1 + 1/2Q}{1 - 1/2Q}\right)^{N-1} \tag{16}$$

and

$$N = 1 + \frac{\ln\left(\frac{f_N}{f_1}\right)}{\ln\left(\frac{1+1/2Q}{1-1/2Q}\right)}. \tag{17}$$

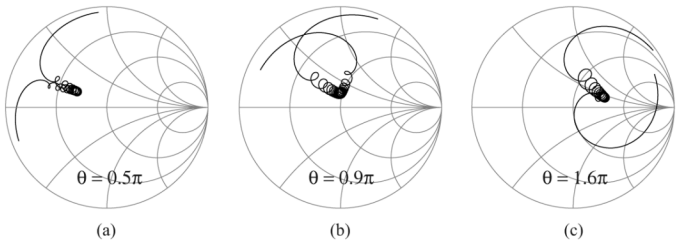

Fig. 4. Channelizer S_{11} for three values of θ. A θ value of 0.9π (b) produces an input return loss of less than -10 dB over the band from 20–90 MHz. The Smith Chart impedance is 50 Ω.

Note that, since the series resonator channel filters are coupled to and loaded by adjacent resonators, each channel filter's loaded Q is less than that of the isolated series resonator. Consequently, one needs to use a slightly larger value of Q in the design process to produce the desired fractional bandwidth channels. For example, as illustrated in Section V, channels with 8.2% fractional bandwidth $(Q = 12.2)$ use resonators with a Q of 15.6 (28% higher). One uses the actual channel filter Q in (17).

B. Determination of Coefficients

The coefficients A_1, A_2, A_3, and α are determined by four design choices, including:

$$\begin{aligned} f_1 &\equiv \text{Lowest channel center frequency;} \\ f_N &\equiv \text{Highest channel center frequency;} \\ \frac{1}{Q} &\equiv \text{Channel fractional bandwidth;} \\ \theta &\equiv \text{Transmisson phase at eachchannel's center frequency.} \end{aligned}$$

The choice of θ is arbitrary, and its value affects the input impedance and overall channelizer response. The design must therefore be simulated with various θ values until the desired response is achieved. Interestingly, the channelizer exhibits a characteristic S_{11} spiral which moves along the real axis of the Smith Chart as one varies θ from zero to values approaching roughly 2π (Fig. 4). The channelizer minimum and maximum channel center frequencies and channel fractional bandwidth are chosen based on the application.

The resonator nearest the channelizer input $(x = 0)$ is tuned at the highest frequency (f_N). Using (8) with $x = 0$ and (11), A_1 is given by

$$A_1 = \frac{1}{(2\pi f_N)^2}. \tag{18}$$

Next, to determine A_2, one uses the desired channel fractional bandwidth and (12) to arrive at

$$A_2 = \frac{\sqrt{A_1}}{Q}. \tag{19}$$

To find α, (8) and (18) are used at the channelizer input $(x = 0)$ and final section $(x = 1)$, where

$$\begin{aligned} x = 1 &\Rightarrow A_1 e^{\alpha} = \frac{1}{(2\pi f_1)^2} \\ x = 0 &\Rightarrow A_1 = \frac{1}{(2\pi f_N)^2} \end{aligned}$$

such that

$$\alpha = \ln\left(\frac{f_N}{f_1}\right)^2. \tag{20}$$

Finally, A_3 is found using a numerical technique and the previously determined constants. The Wentzel–Kramers–Brillouin (W.K.B.) approximation suggests that, if $g(x)$ changes slowly enough with x, then we can approximate the solution to

$$\frac{d^2}{dx^2}u(x) + g(x) \cdot u(x) = 0 \tag{21}$$

at some $x = x_0$ by the solution

$$u(x_0) = U_0 e^{j\int \sqrt{g(x)}dx} = U_0 e^{j\theta}. \tag{22}$$

Comparing (21) with (6), we let

$$g(x) = \frac{L_1(x)C(x)}{1 + j\omega R(x)C(x) - \omega^2 L_2(x)C(x)}\omega^2$$

and

$$u(x) = V(x).$$

Thus, we can find the phase of (22) using

$$\theta \approx \int_0^{x_0} \sqrt{g(x)}\, dx. \tag{23}$$

In (23), θ is the phase of $u(x)$ at location x_0 which is the location of a resonator with a center frequency f_0. The transmission phase at the center frequency of each resonator θ is assumed to be constant in analogy with physiological cochlear response data [13], [14].

Having found A_1, A_2, and α, and choosing a value of θ, (23) is numerically integrated along the channelizer length (x) for each value of x_0. For each point x_0 along x an integral is evaluated and the needed term $L_1(x)C(x)$ is found. The result is an arbitrary function which is then fit to the desired form of (10), giving the value of A_3.

Having found the four constants A_1, A_2, A_3, and α, each circuit component of the constant fractional bandwidth channelizer is determined from (8) to (10). In our designs, the value of $R(x)$ is made constant for each resonator section to ensure a constant impedance at each output port. Therefore, first $C(x)$ is determined from (9), and then $L_1(x)$ and $L_2(x)$ are calculated from (10) and (8).

C. Constant Absolute Bandwidth Formulation

In many cases, a channelizer filter with a constant absolute bandwidth (Δf) outputs is needed. In this case, the number of channels needed to cover a specified bandwidth is given by

$$N = 1 + \frac{f_N - f_1}{\Delta f}. \tag{24}$$

Such a channelizer results from modifying the functional dependence of the channel center frequencies from exponential to linear.

For a constant channel bandwidth, the channel center frequencies are given by

$$f_0 = B_1 + B_2 x. \tag{25}$$

Equating this with the resonant frequency of a series *LCR* resonator results in

$$L_2(x)C(x) = \frac{1}{\left[2\pi\left(B_1 + B_2 x\right)\right]^2}. \tag{26}$$

Using (25) and (26) in (12), we obtain

$$R(x)C(x) = \frac{\Delta f}{2\pi\left(B_1 + B_2 x\right)^2}. \tag{27}$$

Combining (26) and (27) leads to

$$L_2(x) = \frac{R(x)}{2\pi\Delta f} \tag{28}$$

and, for resonators with identical output impedance $(R(x))$, the resonator inductance value $(L_2(x))$ is also fixed and inversely proportional to the channel bandwidth. Note that this relationship places a practical restriction on the realizable bandwidth of the constant absolute bandwidth design, for a given channel bandwidth, due to inductor parasitics: the channelizer's maximum frequency must be below the inductor's self-resonant frequency.

Suggested by the form of (27), the last relationship among the circuit elements is chosen as

$$L_1(x)C(x) = \frac{1}{\left[2\pi\left(B_3 + B_4 x\right)\right]^2}. \tag{29}$$

This was found empirically to result in a channelizer with constant absolute bandwidth channels as well as a good input impedance match over the entire channelizer bandwidth.

D. Determination of Coefficients

For the channelizer with constant absolute bandwidth channels, the coefficients B_1, B_2, B_3, and B_4 are determined from the chosen values of:

$f_1 \equiv$ Lowest channel center frequency;
$f_N \equiv$ Highest channel center frequency;
$\Delta f \equiv$ Channel absolute bandwidth;
$\theta \equiv$ Transmission phase at eachchannel's center frequency.

Since the highest frequency resonator appears at the channelizer input $(x = 0)$, using (25), we find that

$$B_1 = f_N. \tag{30}$$

At the lowest frequency resonator $(x = 1)$, again using (25), we find that

$$B_2 = f_1 - f_N. \tag{31}$$

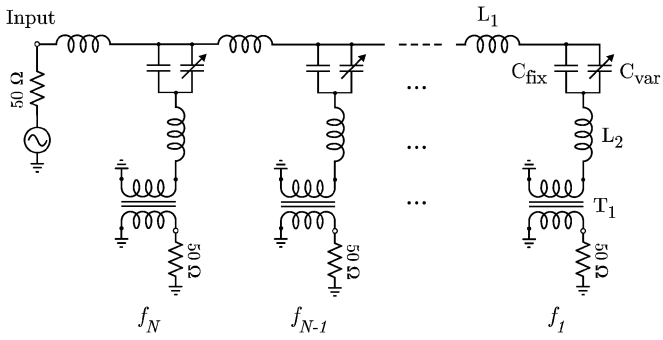

Fig. 5. Schematic diagram of the channelizer prototypes. In this implementation, the resonator capacitances are formed by the parallel combination of $C_{\rm fix}$ and $C_{\rm var}$ to allow fine tuning.

Finally, the constants B_3 and B_4 are determined by using the same numerical integration and curve-fitting procedure used in the constant fractional bandwidth design. However, in the constant absolute bandwidth case, (29) is substituted in the kernel $g(x)$ of (23). Again here, the choice of the phase at each center channel (θ) is adjusted by trial-and-error in simulation to optimize channelizer input return loss.

Having found B_1, B_2, B_3, and B_4, the channelizer circuit elements are determined. With $R(x)$ constant, $L_2(x)$ is given by (28), $C(x)$ is found using (26), and $L_1(x)$ is given by (29).

V. Experimental Results

Two channelizer prototypes were designed, built, and measured to demonstrate the cochlea-inspired channelizer topology. Each circuit was realized in a modified version of the discretized transmission-line model as shown in Fig. 5. As shown later in simulated and measured results, this discretization results in ripples in the filter transmission and reflection.

In the first built versions of the channelizer, component and printed circuit board (PCB) parasitics caused unwanted in-band resonances, emphasizing the need for accurate simulation. For the prototypes presented here, circuit simulations were performed in Agilent ADS 2005A[1] using manufacturer-provided S-parameters of all lumped components except for the RF transformers. The RF transformer S-parameter blocks were generated from a de-embedded fixture measurement. Board parasitics were accounted for using an S-parameter block derived from a full-wave Sonnet *em* model.[2] The resulting simulations accurately predicted parasitic resonances.

A. Constant Fractional Bandwidth Channelizer

A 20-channel channelizer with constant fractional bandwidth channels covering 20–90 MHz is shown in Fig. 6.

The series inductances L_1 are air-wound inductors (Coilcraft Midi Spring) with Q of 60–100 over the channelizer bandwidth. The shunt resonator sections are designed for a loaded Q of 16 and $|X_L| = |X_C| = 200\ \Omega$ at resonance, resulting in an effective impedance of 12.5 Ω. This is transformed to 50 Ω through a 1:2 turns ratio RF transformer (Coilcraft TTWB) at

[1]ADS 2005A, Agilent Technologies, Inc., Palo Alto, CA, 2005.

[2]Sonnet, Version 10.52, Sonnet Software, Inc., North Syracuse, NY, 2005.

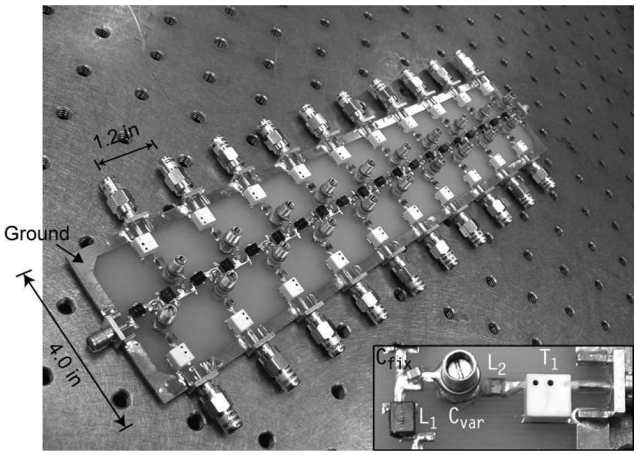

Fig. 6. Photograph of the 20-channel, 20–90 MHz channelizing filter with constant fractional bandwidth channels. The inset shows a single channel layout (from [3]).

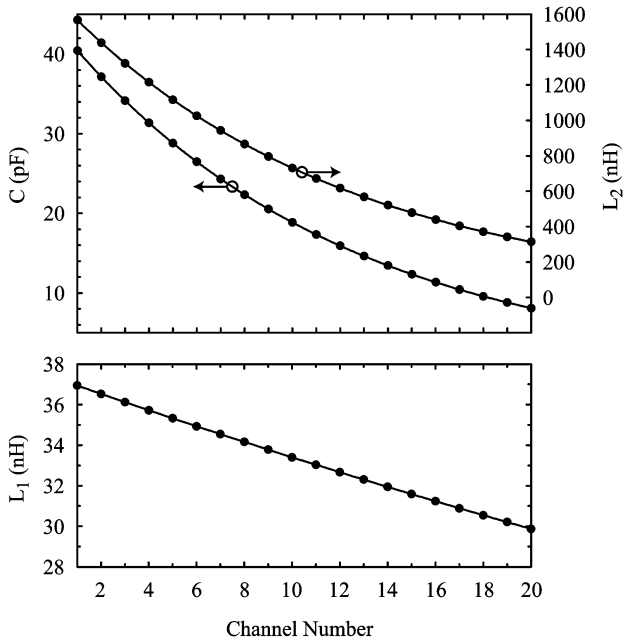

Fig. 7. Component values for L_1, L_2, and C for the 20–90-MHz constant fractional bandwidth (8%) channelizer (from [3]).

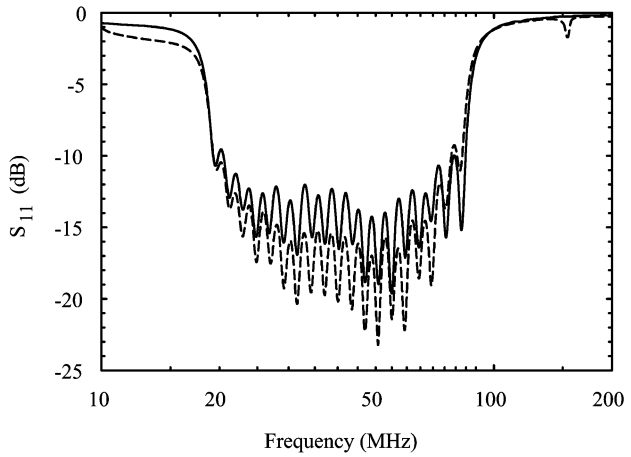

Fig. 8. Measured (solid line) and simulated (dashed line) S_{11} of the 20-channel constant fractional bandwidth channelizer (from [3]).

each channel output. The shunt resonator inductors L_2 (Coilcraft 0805CS) are ceramic body wire-wound surface-mount components with Q of 25–40 at the channel center frequencies. To take into account the tolerance in the component values and since the capacitors and inductors are commercially available in discrete values, the resonator capacitances C are implemented with the parallel combination of a fixed surface-mount capacitor (ATC 600F) and a coaxial trimmer capacitor (Sprague GAA). The trimmer capacitor was included to ease the tolerance requirement of the other components—a design using all fixed-value components $(\pm 2\%)$ is certainly possible. The total capacitor Q is greater than 200 over the channelizer bandwidth. Channelizer component design values range from 30 to 37 nH for L_1, 310 to 1570 nH for L_2, and 8 to 40 pF for C (Fig. 7). The circuit is constructed on a 61 mil FR-4 PCB (Fig. 6) with the ground located along the perimeter of the PCB to reduce shunt parasitic capacitance. Simulations on two-sided PCB identified significant layout parasitics that gave undesirable spurious responses within the filter passband.

B. Measurements

The channelizer is tuned by adjusting the trimmer capacitors on individual channel resonators until nulls in the measured S_{11} match the simulated response (Fig. 8). The tuning procedure involved first setting each trimmer at maximum capacitance and then adjusting for the desired response by lowering the appropriate trimmer value beginning with the highest frequency channel. Channelizer measured and simulated S_{21} for each channel ($S_{(n+1)1}$ for $1 \leq n \leq 20$) are shown in Fig. 9. Measured insertion loss at the center of each channel ranges from 2.5 to 5.3 dB, with an average of 4.8 dB.

A sample of three separate channel responses is shown in Fig. 10. Focusing on channel 10, we notice the characteristic cochlear response. The passband slope is first-order (20 dB/decade) below the channel center frequency and over fifth-order (100 dB/decade) immediately above the channel center frequency due to the low-pass nature of the dispersive transmission line. Note that, for frequencies outside of the channelizer bandwidth, each channel has a characteristic single LCR response. This can be seen as an increase in S_{21} for all channels beginning at both 20 and 90 MHz. Also, the self-resonance of the resonator inductors produces a parasitic resonance at 150 MHz. The measured center frequencies and channel responses match simulation closely. Adjacent channel S_{21} cross at approximately 2 dB below each channel's center frequency (Table I). Each channel's 2-dB crossover bandwidth is $8.2 \pm 0.1\%$. Spurious responses above 100 MHz are due to resonances of the lumped inductors as well as PCB parasitic shunt capacitance.

To understand the channelizer loss, consider the power distribution at the center frequency of channel 10 (39.4 MHz) (Table II). The percent of the input power appearing at the individual outputs is calculated from each channel's measured $|S_{21}|^2$. Likewise, the reflected power at the channelizer input is given by $|S_{11}|^2$. At 39.4 MHz, 33.2% of the power arrives

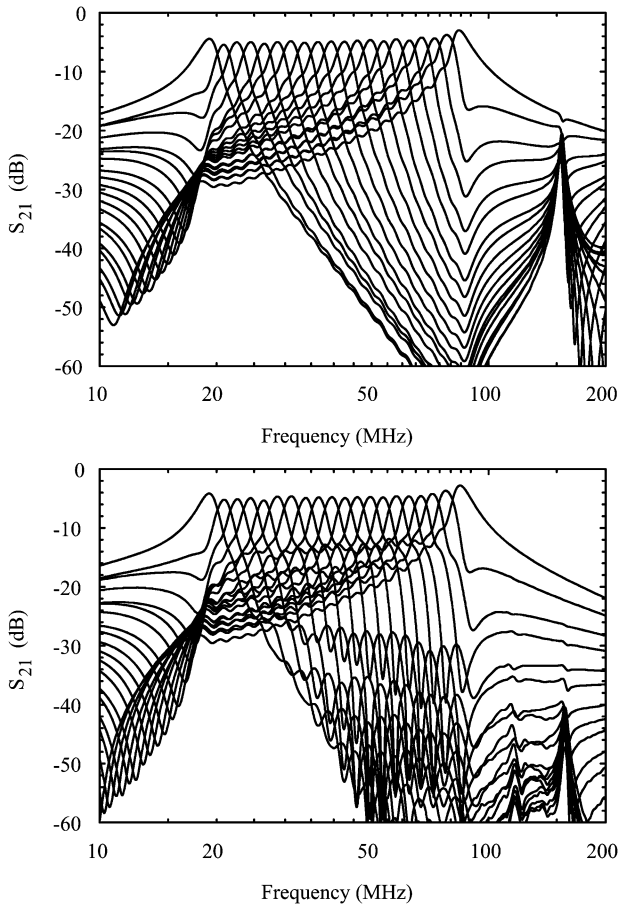

Fig. 9. Simulated (top) and measured (bottom) S_{21} for each channel of the channelizing filter (from [3]).

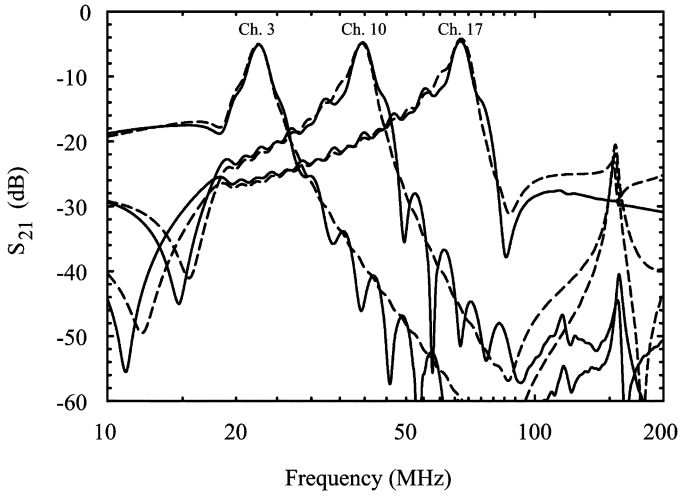

Fig. 10. Measured (solid line) and simulated (dashed line) S_{21} of the constant fractional bandwidth channelizer for channels 3 (22.5 MHz), 10 (39.4 MHz), and 17 (67.3 MHz). Ripples are due to parasitics and resonances of the lumped components (from [3]).

at the channel-10 output (-4.8 dB), 32.3% appears at all other channel outputs (Fig. 11), and 3.5% is reflected at the channelizer input. Summing the powers results in 69.0% of

TABLE I
CHANNELIZER CENTER FREQUENCIES (IN MEGAHERTZ)

Ch	f_c	Ch	f_c	Ch	f_c	Ch	f_c
1	19.2	6	28.7	11	42.4	16	62.4
2	20.8	7	31.1	12	46.0	17	67.3
3	22.5	8	33.5	13	49.6	18	72.6
4	24.4	9	36.3	14	53.8	19	78.2
5	26.5	10	39.4	15	58.0	20	84.3

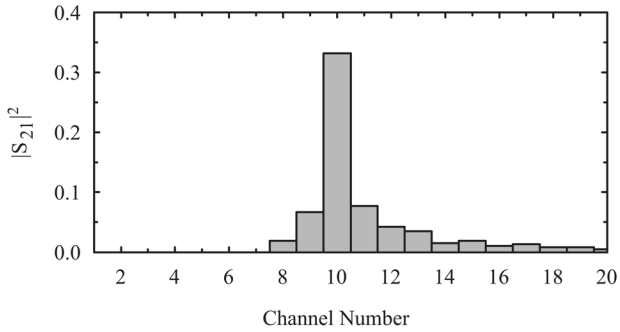

Fig. 11. Measured power distribution at the center frequency of channel 10 (39.4 MHz) among all 20 channels (from [3]).

TABLE II
SAMPLE CHANNEL POWER DISTRIBUTION FOR CHANNEL 10

	Power (%)
Channel 10 Output	33.2 (-4.8 dB)
Sum of Channel 1–9, 11–20 Outputs	32.3
Reflected at Input	3.5
Sum of all Power Contributions	69.0
Power Dissipated	31.0

the input power. Thus, the filter dissipates 31.0% of the input power corresponding to an effective loss of 1.6 dB.

C. Constant Absolute Bandwidth Channelizer

The 20-channel channelizer with constant absolute bandwidth channels covering roughly 20–90 MHz is shown in Fig. 13.

This design also uses high-Q surface-mount components throughout, with air-coil inductors for both L_1 and L_2 (Coilcraft Midi and Maxi Spring). In contrast to the constant fractional bandwidth case, the individual channel resonators have a loaded Q that varies with resonator center frequency, producing constant absolute channel bandwidth. The resonators are again designed for a series resistance, at resonance, of 12.5 Ω and 1:2 turns ratio RF transformers (Coilcraft WB1040) are used at each channel output to produce a 50-Ω output impedance. The resonator capacitances C also employ a parallel combination of a fixed capacitor (ATC 600F) and a coaxial trimmer capacitor (Sprague GAA) to allow for fine-tuning channel center frequencies. Channelizer component design values range from 19 to 296 nH for L_1 and 5 to 150 pF for C, while L_2 is fixed at 422 nH (Fig. 12).

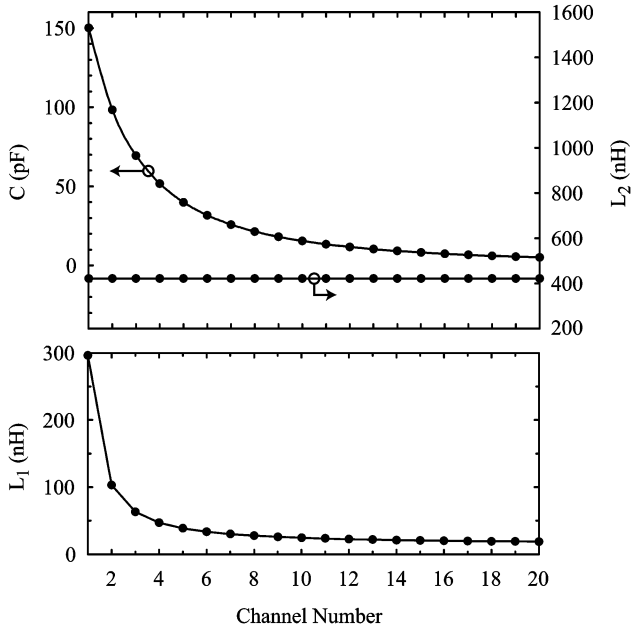

Fig. 12. Component values for L_1, L_2, and C for the 20–90-MHz constant absolute bandwidth channelizer.

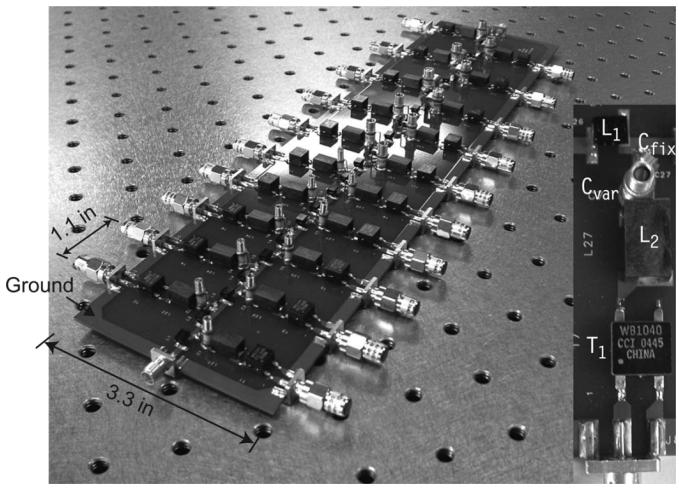

Fig. 13. Photograph of the 20-channel, 20–90-MHz channelizing filter with constant absolute bandwidth channels. The inset shows a single channel layout.

D. Measurements

The channelizer is tuned by adjusting the trimmer capacitors on individual channel resonators until nulls in the measured S_{11} match the simulated response (Fig. 14) assuring the correct resonator center frequencies. Measured and simulated S_{21} for each channel ($S_{(n+1)1}$ for $1 \leq n \leq 20$) are shown in Fig. 15 while a sample of three separate measured channel responses is shown in Fig. 16 showing good agreement with simulations. Measured insertion loss at the center of each channel ranges from 1.9 to 4.8 dB, with an average of 4.3 dB. The measured center frequencies and channel responses again match simulation closely. As in the constant fractional bandwidth case, adjacent channel S_{21} responses cross at ~ 2 dB below each channel's center frequency (Table III). Each channel's 2-dB crossover bandwidth is a nearly constant 4 MHz, resulting in fractional bandwidths ranging from 26.0% (channel 1) to 4.3% (channel 20).

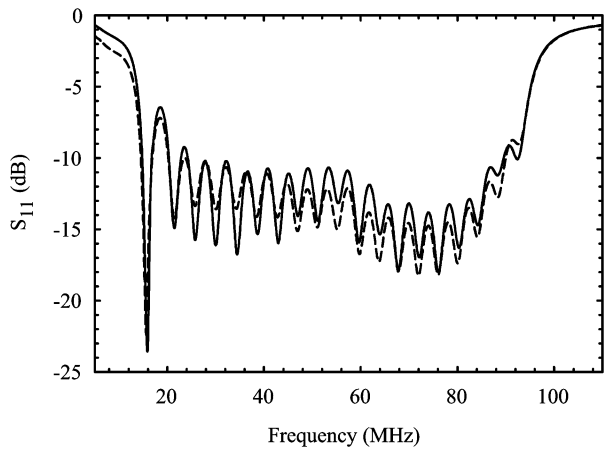

Fig. 14. Measured (solid line) and simulated (dashed line) S_{11} of the 20-channel constant absolute bandwidth channelizer.

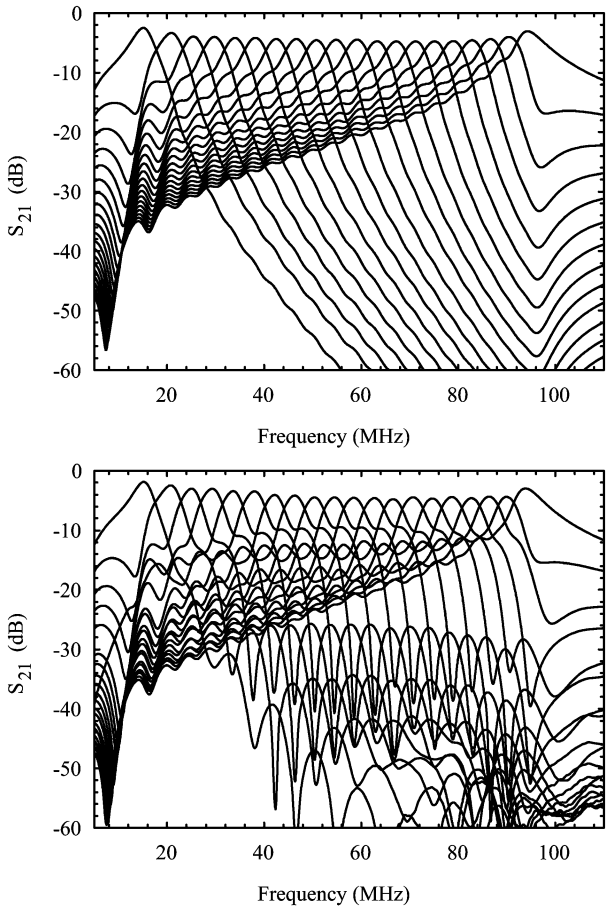

Fig. 15. Simulated (top) and measured (bottom) S_{21} for each channel of the constant absolute bandwidth channelizing filter. The frequency scale is linear to show the constant absolute bandwidth response.

The power distribution at the center frequency of channel 10 (54.5 MHz) is shown in Table IV. The percent of the input power appearing at the individual outputs is calculated from each channel's measured $|S_{21}|^2$ and the reflected power at the channelizer input is given by $|S_{11}|^2$. At 54.5 MHz, 35.4% of the power arrives at the channel 10 output (-4.5 dB), 39.8%

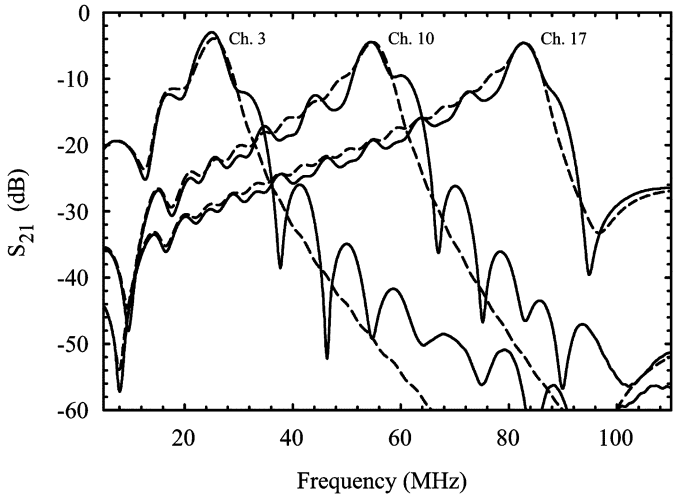

Fig. 16. Measured (solid line) and simulated (dashed line) S_{21} of the constant absolute bandwidth channelizer for channels 3 (25.1 MHz), 10 (54.5 MHz), and 17 (82.6 MHz).

TABLE III
CHANNELIZER CENTER FREQUENCIES (IN MEGAHERTZ)

Ch	f_c	Ch	f_c	Ch	f_c	Ch	f_c
1	15.4	6	37.8	11	58.5	16	78.6
2	20.5	7	42.4	12	62.5	17	82.6
3	25.1	8	46.4	13	66.5	18	86.7
4	29.2	9	50.4	14	70.6	19	90.1
5	33.8	10	54.5	15	74.6	20	93.6

TABLE IV
SAMPLE CHANNEL POWER DISTRIBUTION FOR CHANNEL 10

	Power (%)
Channel 10 Output	35.4 (−4.5 dB)
Sum of Channel 1–9, 11–20 Outputs	39.8
Reflected at Input	5.8
Sum of all Power Contributions	81.0
Power Dissipated	19.0

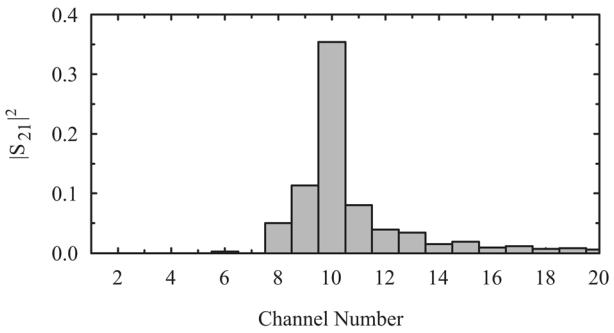

Fig. 17. Measured power distribution at the center of channel 10 (54.5 MHz) among all 20 channels.

appears at all other channel outputs (Fig. 17), and 5.8% is reflected at the channelizer input. Summing the powers results in 81.0% of the input power. Thus, the filter dissipates 19.0% of the input power corresponding to an effective loss of 0.9 dB.

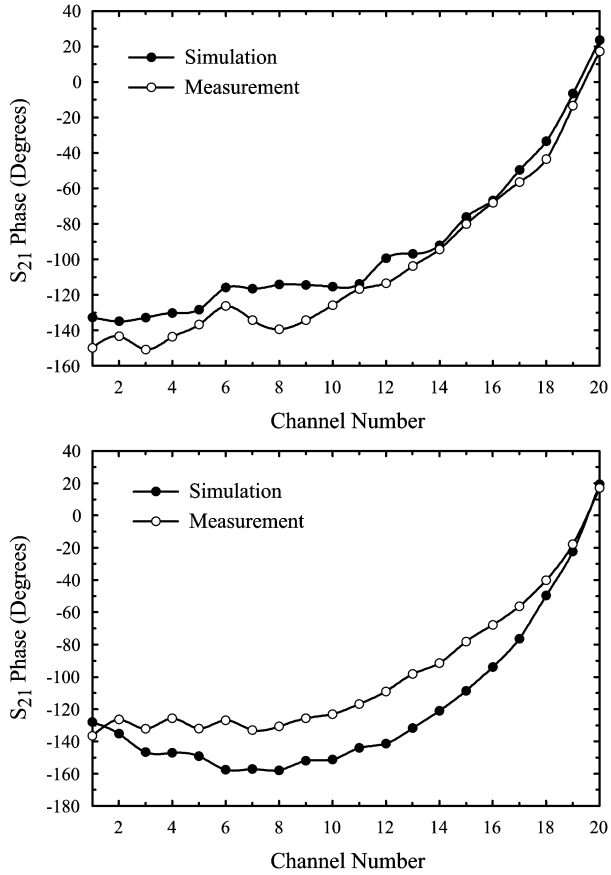

Fig. 18. Measured and simulated phase of S_{21}, at each channel's center frequency, for the constant fractional bandwidth version (top) and the constant absolute bandwidth version (bottom). The data for each channel is taken at the center frequency of the particular channel.

VI. DISCUSSION

A. Channel Phase Response

From the results presented so far, we see that a channelizing filter based on cochlear modeling produces channels with near-uniform amplitude response; a characteristic $|S_{21}|$ scaled in frequency from one channel to the next. In addition, from data on biological cochlea measurements, we expect that the phase of S_{21} at each center frequency is nearly identical for all channels [13], [14]. This is shown in measured and simulated results for the RF channelizers (Fig. 18).

The uniformity among channel response in amplitude, phase, and phase constancy at the center frequency is determined by the number of sections physically preceding a particular channel. Typically, a minimum of five sections are needed to set up the characteristic response. Since these initial sections are the higher frequency channels, the lower frequency sections of the channelizer have the most uniform response.

B. Transient Response

In many situations, it is desirable to decompose a wideband input signal into narrower channels in real time. Transient simulations were done to demonstrate this channelizing filter's capability in such a system. These simulations were performed using

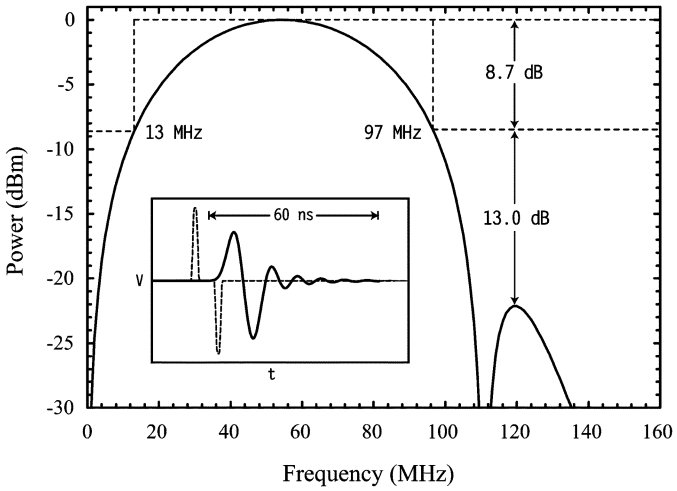

Fig. 19. Simulated spectrum of the bandlimited input signal used in the time-domain simulation (power adjusted to deliver 0 dBm at the band center). The inset shows the waveforms of prefilter input monopulse (dashed line) and the bandlimited signal (solid line) that is fed to the channelizer input.

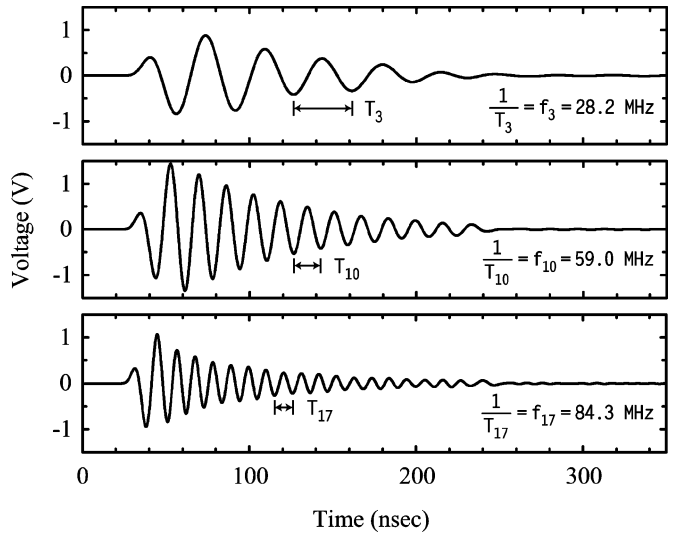

Fig. 20. Three representative simulated waveforms that appear at channelizer output ports with the input signal shown in Fig. 19.

the constant absolute bandwidth channelizer. Finite Q, but otherwise ideal lumped elements were used to reduce transient simulation complexity. Because the simulation did not include component or board parasitics, the channel responses were shifted slightly up in frequency compared with the previous S-parameter simulations.

A Gaussian monopulse filtered through a high-order maximally flat filter was used to simulate a signal with a spectrum concentrated in the channelizer bandwidth (Fig. 19). A sample of the channel outputs is shown in Fig. 20. As expected, each waveform is an exponentially decaying sinusoid of a frequency centered in the respective channel's passband. Thus, this type of channelizer can be used in a pulsed wideband receiver where simultaneous reception is desired on every channel.

C. Enhancements for Radio Systems

The cochlea has been the subject of intense modeling effort since the 1950s. Most of this research has focused on understanding mammalian cochlear dynamics. In this work, our focus has been to adapt the cochlear structure to radio frequencies where we so often require channelization. To this end, the next obvious step is to increase the order of each channel's filter section to provide even more adjacent channel rejection.

In theory, the cochlea-inspired channelizer topology can be applied to any frequency range. Implementing the design at microwave frequencies is currently being done with printed lumped elements as well as distributed filter sections, with promising results so far [15]. One obvious limitation is the effect of lumped component (especially inductor) self-resonances which produce undesirable responses within the total channelizer bandwidth. For channelizers covering many octaves, one must also mitigate the harmonic responses of distributed filter sections.

The cochlea-inspired channelizer circuit is a wide bandwidth contiguous channel multiplexer with a large number of channels. Conventional manifold type RF and microwave multiplexers using high-Q resonator technologies can achieve lower insertion loss and arbitrary pass-band responses, but with a limited number of channels (due to design complexity). Such high performance filters also come with a high cost and large size. In applications such as receiver front-end preselection and instantaneous spectrum monitoring, where lower stop-band rejection can be traded for a large number of channels, a cochlea-like channelizer fulfills the need with a straightforward design method.

VII. Conclusion

A new type of RF channelizing filter based on a simplified model of the mammalian cochlea has been demonstrated. Versions of the filter offer channels with either constant fractional or constant absolute bandwidth. The filter topology is scalable to any frequency, with the frequency coverage limited by out-of-band resonator response. A design methodology is also presented.

Acknowledgment

Opinions, interpretations, conclusions, and recommendations are those of the author(s) and are not necessarily endorsed by the United States Government.

References

[1] I. Hunter, L. Billonet, B. Jarry, and P. Guillon, "Microwave filters—Applications and technology," *IEEE Trans. Microw. Theory Tech.*, vol. 50, no. 3, pp. 794–805, Mar. 2002.

[2] C. Rauscher, "Efficient design methodology for microwave frequency multiplexers using infinite-array prototype circuits," *IEEE Trans. Microw. Theory Tech.*, vol. 42, no. 7, pp. 1337–1346, Jul. 1994.

[3] C. Galbraith, R. White, K. Grosh, and G. M. Rebeiz, "A mammalian cochlea-based RF channelizing filter," in *IEEE MTT-S Int. Microw. Symp. Dig.*, Jun. 2005, pp. 1935–1938.

[4] P. Dallos, A. Popper, and R. Fay, "The cochlea," in *Springer Handbook of Auditory Research*. New York: Springer, 1996, vol. 8.

[5] A. Parthasarathi, "Numerical modeling and electro-acoustic stimulus response analysis for cochlear mechanics," Ph.D. dissertation, Dept. Mech. Eng., Univ. of Michigan, Ann Arbor, MI, 2000.

[6] C. D. Geisler, *From Sound to Synapse: Physiology of the Mammalian Ear*. New York, NY: Oxford Univ. Press, 1998.
[7] L. Watts, "Cochlear mechanics: Analysis and analog VLSI," Ph.D. dissertation, Dept. Elect. Eng., California Inst. of Technol., Pasadena, 1993.
[8] J. Lazzaro, "Circuit models of sensory transduction in the cochlea," in *Analog VLSI Implementation of Neural Systems*, C. Mead and M. I. Ismail, Eds. New York: Springer-Verlag.
[9] S. M. Zhak, S. Mandal, and R. Sarpeshkar, "A proposal for an RF cochlea," in *Proc. Asia Pacific Microw. Conf.* , New Delhi, India, Dec. 2004 [Online]. Available: http://riotact.mit.edu/writings/apmc2004.pdf
[10] S. Mandal, S. M. Zhak, and R. Sarpeshkar, "Circuits for an RF cochlea," in *IEEE ISCAS Int. Symp. Dig.*, May 2006, pp. 3610–3613.
[11] E. d. Boer and E. v. Bienema, "Solving cochlear mechanics problems with higher-order differential equations," *J. Acoust. Soc. Amer.*, vol. 72, no. 5, pp. 1427–1434, 1982.
[12] A. Parthasarathi, K. Grosh, and A. Nuttall, "Three-dimensional numerical modeling for global cochlear dynamics," *J. Acoust. Soc. Amer.*, vol. 107, no. 1, pp. 474–485, 2000.
[13] T. Ren, "Longitudinal pattern of basilar membrane vibration in the sensitive cochlea," in *Proc. Nat. Acad. Sci.*, 2002, vol. 99, pp. 17101–17106.
[14] L. Robles and M. A. Ruggero, "Mechanics of the mammalian cochlea," *Physiol. Rev.*, vol. 81, pp. 1305–1352, 2001.
[15] C. Galbraith, G. M. Rebeiz, and R. Drangmeister, "A cochlea-based preselector for uwb applications," in *IEEE RFIC Symp. Dig.*, Jun. 2007, pp. 219–222.

Christopher J. Galbraith (S'00) received the B.S.E.E. and M.S.E.E. degrees from the University of Michigan, Ann Arbor, where he is currently working toward the Ph.D. degree.

During the summers of 2002 and 2003, he was an intern with TRW Space and Electronics, Redondo Beach, CA, where he worked on satellite communications systems and microwave circuit design. His research interests include RF and microwave circuits, antennas, and systems.

Mr. Galbraith was the recipient of a University of Michigan EECS Department Fellowship in 2003 and received the University's Richard K. Brown Award in 2005.

Robert D. White (M'05) received the B.S. and M.S. degrees from the Massachusetts Institute of Technology, Cambridge, in 1999, and the Ph.D. degree from the University of Michigan, Ann Arbor, in 2005, all in mechanical engineering.

His doctoral research focused on adapting the ideas of cochlear mechanics to the design of lifesize micromachined cochlear models and cochlear-like sensors. He is currently an Assistant Professor of Mechanical Engineering with Tufts University, Medford, MA. His research interests include microsystems, particularly acoustic sensors, microfabrication, and cochlear mechanics.

Dr. White was the recipient of the National Science Foundation Graduate Research Fellowship and a Rackham Fellowship while at Michigan. He was a recipient of the Draper Fellowship and worked at the C.S. Draper Laboratories on MEMS gyroscopes from 1996 to 2000.

Lei Cheng received the B.S. and M.S. degrees in engineering mechanics from Tsinghua University, Beijing, China, in 2000 and 2002, respectively, and the Ph.D. degree in mechanical engineering from the University of Michigan, Ann Arbor, in 2007.

Between 2000 and 2002, her research interests were the modeling of thermomechanical properties of short-fiber reinforced metal matrix composites (MMCs). Since 2003, her research interests have been cochlear modeling and the design of electroacoustic transducers.

Dr. Cheng was the recipient of a University Fellowship at Michigan.

Karl Grosh received the B.S. and M.S. degrees in engineering science from The Pennsylvania State University, University Park, in 1985 and 1988, respectively, and the Ph.D. degree in mechanical engineering from Stanford University, Stanford, CA, in 1994.

He was a Research Scientist with the Naval Research Laboratory, Washington, DC, from 1987 to 1990. Since 1994, he has been a faculty member with the University of Michigan, Ann Arbor, where he is currently an Associate Professor of Mechanical Engineering with a dual appointment in the Biomedical Engineering Department. His current research interests are in cochlear mechanics, the biomechanics of growth, and the design and fabrication of electroacoustic transducers.

Prof. Grosh is a member of the Acoustical Society of America, the American Society of Mechanical Engineers, and the Association for Research in Otolaryngology. He was the recipient of the National Science Foundation Career Award in 1999 and the Office of Naval Research Young Investigator Award in 1999.

Gabriel M. Rebeiz (F'97) received the Ph.D. degree from the California Institute of Technology, Pasadena.

He is currently a Professor of electrical engineering with the University of California, San Diego. Prior to this appointment, he was at the University of Michigan, Ann Arbor, from 1988 to 2004. He has contributed to planar millimeter-wave (mm-wave) and terahertz antennas and imaging arrays from 1988 to 1998 and to the development of RF MEMS from 1996 to present. He is the author of the book *RF MEMS: Theory, Design and Technology* (Wiley: 2003). His group recently developed the fastest mm-wave SiGe switch to date (70 ps) and 6–18 GHz and 30–50 GHz eight-and 16-element phased array receivers and transmitters on a single chip, making them the most complex RFICs ever built at this frequency range. He leads a group of 18 Ph.D. students and three post-doctoral fellows at UCSD in the area of mm-wave RFIC, microwaves circuits, RF MEMS, planar mm-wave antennas and terahertz systems.

Prof. Rebeiz is a National Science Foundation Presidential Young Investigator, an URSI Koga Gold Medal Recipient, and an IEEE MICROWAVE THEORY AND TECHNIQUES (MTT) Distinguished Young Engineer (2003). He was the recipient of the IEEE MTT Society 2000 Microwave Prize along with the College of Engineering Teaching Award, the 1998 Eta-Kappa-Nu Professor of the Year Award, and the 1998 Amoco Teaching Award given to the best undergraduate teacher, all at the University of Michigan. He has been an Associate Editor of the IEEE TRANSACTIONS ON MICROWAVE THEORY AND TECHNIQUES (2000–2003) and a Distinguished Lecturer for IEEE MTT and IEEE Antennas and Propagation Societies.